

ABAQUS implementation of coupled hydrogen diffusion

Emilio Martínez-Pañeda^{a,*}

^a*Department of Civil and Environmental Engineering, Imperial College London, London SW7 2AZ, UK*

Abstract

Documentation that accompanies the file UMATHTH.f - a combination of ABAQUS user subroutines (UMATHHT + UMAT + UEXTERNALDB) to model coupled mechanical deformation and hydrogen diffusion, including multi-trapping. If using this code for research or industrial purposes, please cite:

R. Fernández-Sousa, C. Betegón, E. Martínez-Pañeda. Analysis of the influence of microstructural traps on hydrogen assisted fatigue. *Acta Materialia* 199: pp. 253-263 (2020)

The files can be downloaded from www.imperial.ac.uk/mechanics-materials and www.empaneda.com, along with many other UEL, UMAT and USDFLD subroutines.

Keywords:

Hydrogen embrittlement, Finite element analysis, Trapping, ABAQUS, Stress-assisted diffusion

1. Introduction

Hydrogen originating from water vapour, aqueous electrolytes or gaseous environments significantly increases cracking susceptibility and fatigue crack growth rates in metals [1, 2]. As a consequence, there is an increasing interest in developing mechanistic models for predicting this so-called hydrogen

*Corresponding author.

Email address: e.martinez-paneda@imperial.ac.uk (Emilio Martínez-Pañeda)

embrittlement phenomenon [3–6].

Hydrogen atoms can reside at interstitial lattice sites and microstructural trapping sites, such as dislocations, grain boundaries, voids, carbides and interfaces. Traps act as hydrogen sinks, slowing diffusion, and are typically characterised by their binding energy W_B and density N_T . The energy barrier that must be overcome for the hydrogen to detrapp increases with $|W_B|$; hydrogen will be strongly retained in deep traps $|W_B| > 60$ kJ/mol but can be easily released from shallow traps $|W_B| < 30$ kJ/mol. Quantifying this partitioning of hydrogen atoms between lattice and trapping sites is of utmost importance in predicting diffusion and embrittlement; see, e.g., [7–9] and references therein.

This report is supplementary to our recent work, Ref. [9], and accompanies UMATHTH.f, a combination of ABAQUS user element subroutines to model hydrogen diffusion and trapping, coupled with mechanical deformation. A comprehensive description of the underlying theoretical model is provided in Section 2, while details of the ABAQUS implementation are given in Section 3. Some readers might wish to jump directly to Section 4, where usage instructions are provided together with a simple validation example. An effort is allocated to provide a very easy to follow description of the underlying theory and the code, accessible for everyone.

2. Hydrogen transport

We deal with transport of diluted species; that is, the concentration of hydrogen is small compared to the concentration of the metal solvent. As a rule of thumb, a mixture containing several species can be considered dilute when the concentration of the solvent is more than 90% mol. Hydrogen atoms occupy normal interstitial lattice sites (NILS) and additionally can reside at trapping sites such as interfaces or dislocations. We adopt the common assumptions of the literature (see, e.g., [10, 11]) and base our modelling on the equilibrium theory presented by Oriani. The subscript L refers to lattice sites and the subscript T to trap sites. It is assumed that traps are isolated (i.e., do not form an extended network). Hence, hydrogen transport between trap sites is by lattice diffusion.

2.1. Hydrogen lattice solubility

In the literature two different but equivalent definitions of the lattice hydrogen concentration C_L can be found, these are described below.

2.1.1. Approach 1: N_L is the density of solvent atoms

One could, as in (e.g.) Ref. [10], define the hydrogen concentration in normal interstitial lattice sites as:

$$C_L = N_L \beta \theta_L \quad (1)$$

where N_L denotes the density of the host metal lattice measured in solvent atoms per unit volume, β is the number of hydrogen atoms that can reside in each lattice site/atom, and θ_L is the lattice occupancy fraction ($0 < \theta_L < 1$). In lay terms, N_L (units of atoms Fe/m³ in steel) is the amount of metal atoms per unit volume, β (units of atoms H/atoms Fe) is the amount of hydrogen atoms that correspond to each metal atom, and θ_L (dimensionless) denotes the amount of these hydrogen sites that have been actually occupied by hydrogen atoms (which is small, $\theta_L \ll 1$, as we are dealing with diluted species). Consequently, the concentration is given in atoms H/m³ (other typical units are wppm or mol H/m³). Thus, both β and N_L are material properties (related to the metal solvent) and θ_L (and consequently C_L) depend on the environment and the diffusion of hydrogen. If V_M is the molar volume of the host lattice expressed in units of volume per lattice mole, one can write

$$N_L = \frac{N_A}{V_M} = \frac{N_A \rho_M}{M_M} \quad (2)$$

where $N_A = 6.022 \times 10^{23}$ atoms per mole is Avogadro's number. As depicted in (2), the molar volume equals the molar mass/atomic weight divided by the density $V_M = M_M/\rho_M$. In the case of iron at 293 K, the density equals $\rho_M = 7.87 \times 10^3$ kg/m³ and the atomic weight $M_M = 55.8 \times 10^{-3}$ kg/mol. This necessarily implies,

$$N_L = \frac{N_A \rho_M}{M_M} = \frac{6.022 \times 10^{23} [\text{at/mol}] \cdot 7.87 \times 10^3 [\text{kg/m}^3]}{55.8 \times 10^{-3} [\text{kg/mol}]} = 8.46 \times 10^{28} [\text{at/m}^3] \quad (3)$$

and one should note that β is typically taken to be equal to 6, as indirect evidence indicates tetrahedral site occupancy rather than octahedral site occupancy at room temperature in α -iron (see [12]). For fcc iron, $\beta = 1$ is usually assumed, resulting from the more favourable octahedral site occupancy ($\beta = 2$ for tetrahedral).

2.1.2. Approach 2: N_L is the density of lattice sites

Alternatively, as in (e.g.) Ref. [12], the lattice hydrogen concentration can be defined as:

$$C_L = N_L \theta_L \quad (4)$$

where N_L denotes instead the number of lattice sites per unit volume. Accordingly, in bcc iron (where $\beta = 6$):

$$\begin{aligned} N_L &= \frac{\beta N_A \rho_M}{M_M} = \frac{6 [\text{sites/at}] \cdot 6.022 \times 10^{23} [\text{at/mol}] \cdot 7.87 \times 10^3 [\text{kg/m}^3]}{55.8 \times 10^{-3} [\text{kg/mol}]} = \\ &= 5.1 \times 10^{29} [\text{sites/m}^3] \end{aligned} \quad (5)$$

In the present implementation we follow this second approach.

2.2. Trapped hydrogen concentration

We have seen that hydrogen dissolved in metals can be divided into two groups: the lattice hydrogen, which moves freely through the lattice, or the trapping hydrogen, which is trapped in microstructural defects such as dislocations, grain boundaries, voids, carbides and interfaces. These *traps* can be reversible or irreversible, and can also be classified as saturable or unsaturable. Reversible traps are those that can immobilize and release hydrogen while irreversible traps are those that absorb hydrogen and prevent it from escaping. However, one should note that the term irreversible is not fundamentally correct but rather pragmatic, as leakage can always take place for a sufficiently long timescale or a sufficiently high temperature. Assuming Oriani's equilibrium (see below), there is a relation between the occupancy of traps and the lattice hydrogen concentration based on the trap binding energy, W_B .

We will consider the case of multiple traps [9]. Thus, the hydrogen concentration in the i th type of trapping site can be defined as:

$$C_T^{(i)} = \theta_T^{(i)} \alpha^{(i)} N_T^{(i)} \quad (6)$$

where N_T is the number of traps per unit volume, α is the number of atom sites per trap and θ_T is the trap occupancy (again, $0 < \theta_T < 1$). Hence, αN_T is the number of trapping sites per unit volume. Some authors (see, e.g., [12]) take α to be equal to 1 (one hydrogen site per trap) while others consider larger values (e.g., $\alpha = 6$ in [13]). These differences are related to

the concept of atom/site and the binding energy. If α denotes the number of sites per trap, then unequivocally $\alpha = 1$ (and N_T tells us how many sites exist). But α may also denote the number of hydrogen atoms that can be stored in each trap (e.g., in a dislocation $\alpha = 30$). However, not all of those atoms will have the same binding energy, so we choose here to adopt $\alpha = 1$ and consider apparent/average binding energies (e.g., $W_B = -20.2$ kJ/mol for a dislocation). It is also quite common to provide the magnitude of the group αN_T and not of each individual component (see, e.g., Ref. [14]). Accordingly, we re-formulate (6) as:

$$C_T^{(i)} = \theta_T^{(i)} N_T^{(i)} \quad (7)$$

where $N_T \equiv N_T \alpha$ is the trap density (trapping sites per unit volume). The total concentration of hydrogen for a system with n traps then reads:

$$C = C_L + C_T^{(1)} + C_T^{(2)} + \dots + C_T^{(n)} = C_L + \sum_i^n C_T^{(i)} \quad (8)$$

Accordingly,

$$\frac{\partial C}{\partial t} = \frac{\partial C}{\partial C_L} \frac{\partial C_L}{\partial t} + \sum_i^n \frac{\partial C}{\partial C_T^{(i)}} \frac{\partial C_T^{(i)}}{\partial t} \quad (9)$$

2.3. Oriani's equilibrium theory

Oriani's equilibrium theory [15] results in a Fermi-Dirac relation between the occupancy of the i th type of trapping sites and the fraction of occupied lattice sites

$$\frac{\theta_T^{(i)}}{1 - \theta_T^{(i)}} = \frac{\theta_L}{1 - \theta_L} K^{(i)}, \quad (10)$$

with $K^{(i)}$ being the equilibrium constant for the i th type of trap with binding energy $W_B^{(i)}$; given by

$$K^{(i)} = \exp\left(\frac{-W_B^{(i)}}{RT}\right). \quad (11)$$

where the trap binding energy W_B (i.e., the energy required for a hydrogen atom to escape a trap site and move into a lattice site) is inherently negative. And the parameters R and T respectively represent the gas constant (8.3144 J mol⁻¹ K⁻¹) and the absolute temperature. Oriani's equilibrium theory can be used when the trap filling kinetics are very rapid, which is usually the case [16]. In other words, this equilibrium argument is realistic when the lattice

diffusion relaxation times are relatively long compared to the time required to replenish or deplete the traps.

The implications of Oriani's equilibrium can be readily quantified. First, note that (10) can be rewritten as,

$$\frac{1}{\theta_L} = \left(\frac{1}{\theta_T^{(i)}} - 1 \right) K^{(i)} + 1 \quad (12)$$

Implying that larger values of K lead to smaller lattice occupancies θ_L , and consequently, a smaller amount of C_L relative to C_T for a fixed total hydrogen concentration C . As shown in (11), the equilibrium constant K increases with (the absolute value of) the binding energy W_B . Hence, deep traps (strong, irreversible) with larger $|W_B|$ will absorb more lattice hydrogen and act as sinks that will slow diffusion. Secondly, note that one can merge (4), (12) and (11), leading to,

$$\frac{N_L}{C_L} = \left(\frac{1}{\theta_T^{(i)}} - 1 \right) \exp\left(\frac{-W_B^{(i)}}{RT}\right) - 1 \quad (13)$$

and one can accordingly choose representative values of θ_T , and plot C_L versus W_B . We do so in Fig. 1 by adopting $N_L = 5.1 \times 10^{29}$ sites/m³, which is an appropriate choice for bcc iron, as discussed before.

It is observed that deep traps (high $|W_B|$): (i) increase the weight of C_T relative to C_L (i.e., absorb more C than weak traps), and (ii) get filled at low C_L levels (i.e., if C_L is high, then $\theta_T \approx 1$). So, as soon as there is hydrogen in the system, the hydrogen atoms will occupy the deep traps, as this is more energetically favourable. These deep traps will get full soon, and the hydrogen will then distribute through the lattice. Examples of deep traps with high binding energies include carbides of alloying elements ($W_B = -72$ kJ/mol) or grain boundaries ($W_B = -48$ kJ/mol) [13]. In contrast, weaker traps are dislocations, where $|W_B|$ is on the order of 20 kJ/mol. As evident from Fig. 1, these shallow traps with binding energies larger than -20 kJ/mol are effectively empty ($\theta_T \approx 0$) unless C_L is very high, on the order of 10 wt ppm (4.68×10^{25} at H/m³) or higher.

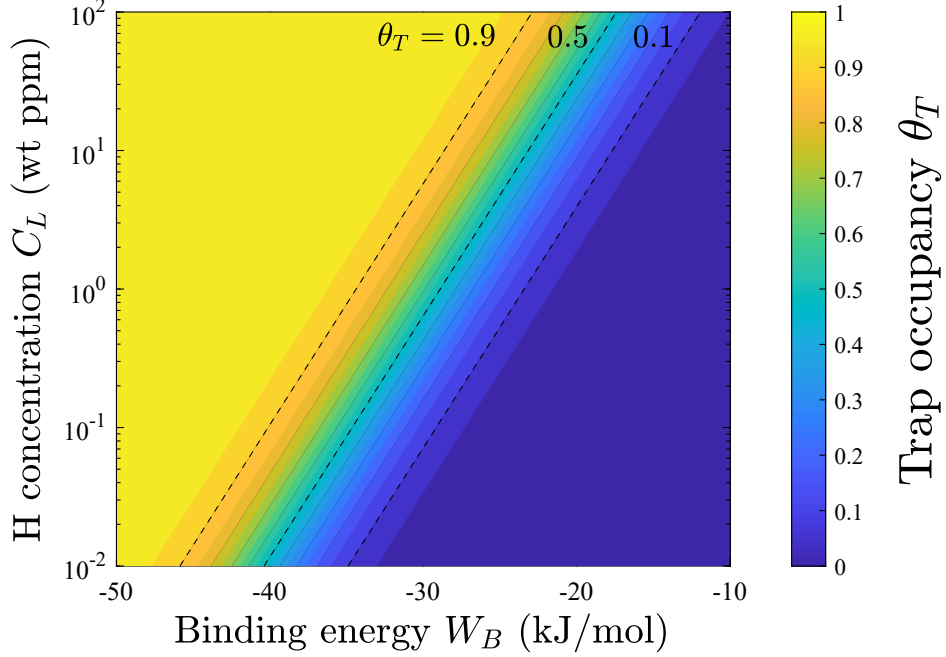


Figure 1: Implications of Oriani's equilibrium; sensitivity of the trap occupancy θ_T to the lattice hydrogen concentration C_L and the trap binding energy W_B . Taken from [9].

In many alloys, especially in bcc lattices, conditions of low occupancy $\theta_L \ll 1$ are usually assumed, because $N_L \gg C_L$, such that

$$\frac{\theta_L}{1 - \theta_L} \approx \theta_L \quad (14)$$

and consequently, by considering (4), (7) and (10)

$$C_T^{(i)} = \frac{K^{(i)} C_L N_T^{(i)} / N_L}{1 + C_L K^{(i)} / N_L} = \frac{K^{(i)} C_L N_T^{(i)}}{N_L + C_L K^{(i)}} \quad (15)$$

which characterizes the equilibrium relationship between C_L and C_T in terms of material parameters. Thus, as the temperature increases and K decreases, the concentration of hydrogen in traps will decrease for a fixed C_L [10, 17]. Finally, some insight into the process of equilibrium trap-filling at fixed temperature and N_T can be obtained by differentiating the previous equation:

$$\frac{\partial C_T^{(i)}}{\partial C_L} = \frac{C_T^{(i)} (1 - \theta_T^{(i)})}{C_L} = \frac{K^{(i)} N_L N_T^{(i)}}{(K^{(i)} C_L + N_L)^2} \quad (16)$$

2.4. Hydrogen diffusion

Even though mass concentration is the sought variable, the thermodynamic driving force for diffusion is the chemical potential gradient $\nabla\mu$. The mass flux is related to $\nabla\mu$ via Onsager coefficients L_{ij} , which denote the action of force j on component i ; a negative sign indicates that the net movement of i -type hydrogen atoms, i.e. hydrogen flux \mathbf{J}_i , occurs from high to low chemical potential regions:

$$\mathbf{J}_i = - \sum_{j=1}^n L_{ij} \nabla\mu_j \quad (17)$$

Such that, for example, considering the lattice sites:

$$\mathbf{J}_L = -L_{LL} \nabla\mu_L \quad (18)$$

One can develop a generalised model account for both lattice and trapping fluxes (see [18]). Here, we follow the common assumption that the mobility between trapping sites is considered close to zero: $D_{TT} \approx 0$, because traps are not connected or because their deep potential energy well prevents hydrogen from diffusing. Hence, only the lattice flux is considered: $\mathbf{J} \equiv \mathbf{J}_L$ and $\mu \equiv \mu_L$. The Onsager coefficient is related to Einstein's equation of diffusion, such that

$$L_{LL} = \frac{D}{RT} C_L \quad (19)$$

where D is the lattice diffusivity, which is understood to be independent of the hydrostatic stress. The chemical potential is given by,

$$\mu = \mu^0 + RT \ln \frac{\theta_L}{1 - \theta_L} - \bar{V}_H \sigma_H \quad (20)$$

where μ_i^0 denotes the chemical potential in the standard state, \bar{V}_H the partial molar volume of hydrogen in solid solution (an overbar usually denotes a partial molar quantity) and σ_H the hydrostatic stress.

Substituting (19)-(20) into (18) gives:

$$\mathbf{J} = -D \frac{C_L}{(1 - \theta_L)} \left(\frac{\nabla C_L}{C_L} - \frac{\nabla N_L}{N_L} \right) + \frac{D}{RT} C_L \bar{V}_H \nabla \sigma_H \quad (21)$$

This expression can be simplified by taking into consideration that the interstitial sites concentration is usually assumed to be constant: $\nabla N_L = 0$. Thus,

$$\mathbf{J} = -D\nabla C_L + \frac{D}{RT} C_L \bar{V}_H \nabla \sigma_H \quad (22)$$

And the derivative of the flux with respect to the lattice hydrogen concentration equals:

$$\frac{\partial \mathbf{J}}{\partial C_L} = \frac{D}{RT} \bar{V}_H \nabla \sigma_H \quad (23)$$

2.5. Mass balance

Fluxes, due to the chemical potential gradient, and hydrogen concentrations are related through the requirement of mass conservation. Thus, in a volume V of surface S and outward normal \mathbf{n} :

$$\frac{d}{dt} \int_V C \, dV + \int_S \mathbf{J} \cdot \mathbf{n} \, dS = 0 \quad (24)$$

where d/dt is the time derivative. For simplicity, let us define the total hydrogen concentration in traps as,

$$C_T = \sum_i C_T^{(i)} \quad (25)$$

Considering the total concentration as $C = C_L + C_T$, the strong form can be readily obtained by making use of the divergence theorem and noting that (24) must hold for any arbitrary volume,

$$\frac{dC_L}{dt} + \frac{dC_T}{dt} = -\nabla \cdot \mathbf{J} \quad (26)$$

By considering (22), one reaches:

$$\frac{dC_L}{dt} + \frac{dC_T}{dt} = D\nabla^2 C_L - \frac{D\bar{V}_H}{RT} \nabla (C_L \nabla \sigma_H) \quad (27)$$

Using Oriani's equilibrium, an effective diffusion coefficient can be defined as:

$$D_e = D \frac{C_L}{C_L + \sum_i C_T^{(i)} (1 - \theta_T^{(i)})}, \quad (28)$$

and the hydrogen transport equation reads

$$\frac{D}{D_e} \frac{\partial C_L}{\partial t} = D \nabla^2 C_L - \nabla \left(\frac{D C_L}{RT} \bar{V}_H \nabla \sigma_H \right), \quad (29)$$

A complete description of the weak form and the corresponding finite element discretization can be found in Ref. [19].

2.6. Dislocation trapping schemes

We have assumed so far that the trap density is a material property that remains constant throughout the analysis. This is appropriate for most trap types but not dislocation trapping sites, as the dislocation density evolves with the applied load. Several schemes have been proposed through the years to capture how the density of dislocation trap sites, $N_T^{(d)}$, evolves with mechanical straining. Laws have been proposed from a purely phenomenological perspective, relating $N_T^{(d)}$ to macroscopic quantities such as the equivalent plastic strain ε^p , but also from a more mechanistic viewpoint, based on dislocation densities ρ . By assuming one trap site per atomic plane threaded by a dislocation, the following relation between the dislocation density ρ and the trap site density $N_T^{(d)}$ can be identified:

$$N_T^{(d)} = \frac{1}{b} \rho \quad (30)$$

where the pre-factor is the inverse of the Burgers vector. In the case of fcc metals it can be expressed as,

$$N_T^{(d)} = \frac{\sqrt{2}}{a} \rho \quad (31)$$

with a being the lattice parameter. Slip in fcc crystals occurs along the close packed plane: specifically, the slip plane (plane of greatest atomic density) is of type $\{111\}$, and the slip direction (close-packed direction within the slip plane) is of type $\langle \bar{1}10 \rangle$. In the bcc case, slip occurs along the plane of shortest Burgers vector as well; however, unlike fcc, there are no truly close-packed planes in the bcc crystal structure. Thus, a slip system in bcc requires heat to activate. Some bcc materials (e.g. α -Fe) can contain up to 48 slip systems. There are six slip planes of type $\{110\}$, each with two $\langle 111 \rangle$ directions (12 systems). There are 24 $\{123\}$ and 12 $\{112\}$ planes each with one $\langle 111 \rangle$ direction (36 systems, for a total of 48). While the $\{123\}$ and

{112} planes are not exactly identical in activation energy to {110}, they are so close in energy that for all intents and purposes they can be treated as identical. For the specific slip plane {110} and direction $\langle 111 \rangle$ we have:

$$N_T^{(d)} = \frac{2}{\sqrt{3}a} \rho \quad (32)$$

where again the Burgers vector corresponds to the inverse of the prefactor. With these considerations, we proceed to describe some of the most commonly used constitutive laws for determining $N_T^{(d)}$ from the deformation state of the material, all of which have been implemented in the code.

2.6.1. Kumnick and Johnson [20] & Sofronis and McMeeking [10]

For models based on the equivalent plastic strain, such as [10, 12, 21], phenomenological expressions are needed to relate $N_T^{(d)}$ and ε^p . A very popular model in the literature since the pioneering work by Sofronis and McMeeking [10], is that by Kumnick and Johnson [20]. They carried out permeation tests on pure iron subjected to hydrogen gas charging and found that the trap density in iron increases sharply with deformations at low deformation levels and then increases more gradually with further deformation. A good fit to their data is given by:

$$\log N_T = 23.26 - 2.33 \exp(-5.5\varepsilon^p) \quad (33)$$

It immediately follows from (33) that,

$$N_T = 10^{23.26 - 2.33 \exp(-5.5\varepsilon^p)} \text{ [sites/m}^3\text{]} \quad (34)$$

One should note that the experiments were conducted in uniaxial conditions, implying that the important role of plastic strain gradients in increasing the dislocation density is not accounted for [3, 22, 23].

2.6.2. Kumnick and Johnson [20] & Krom *et al.* [12]

Krom *et al.* [12] argue that a factor depending on the strain rate should be included to ensure a correct hydrogen balance. Consider for simplicity a one-trap model. As the concentration of trapped hydrogen C_T depends on the trap density N_T , and the latter depends on the plastic deformation, by means of the chain rule one reaches:

$$\frac{\partial C_T}{\partial t} = \frac{\partial C_T}{\partial C_L} \frac{\partial C_L}{\partial t} + \frac{\partial C_T}{\partial N_T} \frac{dN_T}{d\varepsilon^p} \frac{\partial \varepsilon^p}{\partial t} \quad (35)$$

Recall that,

$$\frac{\partial C_T}{\partial C_L} = \frac{C_T(1 - \theta_T)}{C_L} \quad (36)$$

and from (7) immediately follows that $\partial C_T / \partial N_T = \theta_T$. Consequently, the partial derivative of the hydrogen concentration in trap sites with respect to time is

$$\frac{dC_T}{dt} = \frac{C_T(1 - \theta_T)}{C_L} \frac{dC_L}{dt} + \theta_T \frac{dN_T}{d\varepsilon^p} \frac{d\varepsilon^p}{dt} \quad (37)$$

The model depicted before can be therefore extended, with (27) being

$$\left(1 + \frac{C_T(1 - \theta_T)}{C_L}\right) \frac{dC_L}{dt} + \theta_T \frac{dN_T}{d\varepsilon^p} \frac{d\varepsilon^p}{dt} = D\nabla^2 C_L - \nabla \left(\frac{DC_L}{RT} \bar{V}_H \nabla \sigma_H \right) \quad (38)$$

or, by making use of the effective diffusion constant,

$$\frac{D}{D_e} \frac{\partial C_L}{\partial t} + \theta_T \frac{dN_T}{d\varepsilon^p} \frac{d\varepsilon^p}{dt} = D\nabla^2 C_L - \nabla \left(\frac{DC_L}{RT} \bar{V}_H \nabla \sigma_H \right) \quad (39)$$

In a similar manner, we can again use the multivariable chain rule to reformulate (9) as:

$$\frac{\partial C}{\partial t} = \frac{\partial C}{\partial C_L} \frac{dC_L}{dt} + \frac{\partial C}{\partial N_T} \frac{dN_T}{d\varepsilon^p} \frac{d\varepsilon^p}{dt} \quad (40)$$

The derivative of the total hydrogen concentration with respect to N_T can be readily obtained from (15),

$$\frac{\partial C}{\partial N_T} = \frac{\partial C_L + \partial C_T}{\partial N_T} = \frac{KC_L}{KC_L + N_L} \quad (41)$$

And finally recall that one should also estimate the term $dN_T/d\varepsilon^p$. The experiments of Kumnick and Johnson [20] were adopted by Krom *et al.* [12]; thus, considering (34), one reaches:

$$\frac{dN_T}{d\varepsilon^p} = \frac{12.815}{10^9} \exp(-5.5\varepsilon^p) 10^{23.26 - 2.33 \exp(-5.5\varepsilon^p)} \ln 10 = 29.5 \exp(-5.5\varepsilon^p) N_T \quad (42)$$

where we have already taken into consideration that, in our implementation, the units used for N_T are sites/mm³.

2.6.3. *Gilman [24] & Dadfarnia et al. [14]*

Sofronis and co-workers (see, e.g., Refs. [14, 25]) have presented a dislocation-based relationship, using (30) and building upon the work of Gilman [24]. The dislocation density, in line length per cubic meter, is related to the plastic strains *via*:

$$\rho = \begin{cases} \rho_0 + \gamma \varepsilon^p & \text{for } \varepsilon^p < 0.5 \\ 10^{16} & \text{for } \varepsilon^p \geq 0.5 \end{cases} \quad (43)$$

where $\rho_0 = 10^{10}$ line length/m³ denotes the dislocation density for the annealed material and $\gamma = 2.0 \times 10^{16}$ line length/m³. The magnitude of γ is obtained experimentally, and differs from other works [26]. A rate-dependent term can also be included as:

$$\frac{\partial C}{\partial t} = \frac{\partial C}{\partial C_L} \frac{dC_L}{dt} + \frac{\partial C}{\partial N_T} \frac{dN_T}{d\rho} \frac{\partial \rho}{\partial t} \quad (44)$$

2.6.4. *Taylor [27] & Fernandez-Sousa et al. [9]*

Martínez-Pañeda and co-workers [4, 9, 28, 29] have shown the plastic strain gradients and geometrically necessary dislocations play a significant role in crack tip mechanics and hydrogen diffusion. Recently, a formulation was presented in Ref. [9] that enables capturing the role of both geometrically necessary dislocations (GNDs) and statistically stored dislocations (SSDs) in hydrogen embrittlement.

Capturing how the trap density for dislocations $N_T^{(d)}$ evolves with the applied load requires estimating the dislocation density ρ . This can be achieved by following Taylor's [27] dislocation model and accordingly relate the shear flow stress to ρ , the shear modulus μ and the Burgers vector b as

$$\tau = 0.5\mu b\sqrt{\rho}. \quad (45)$$

The dislocation density ρ comprises the sum of the density ρ_{SSD} for statistically stored dislocations (SSDs) and the density ρ_{GND} for geometrically necessary dislocations (GNDs):

$$\rho = \rho_{SSD} + \rho_{GND}. \quad (46)$$

The GND density is defined by:

$$\rho_{GND} = \bar{r} \frac{\eta^p}{b}, \quad (47)$$

where \bar{r} is the Nye-factor and η^p is the effective plastic strain gradient, which is defined as follows [22, 30]:

$$\eta^p = \sqrt{\frac{1}{4}\eta_{ijk}^p\eta_{ijk}^p} \quad \text{with } \eta_{ijk}^p = \varepsilon_{ik,j}^p + \varepsilon_{jk,i}^p - \varepsilon_{ij,k}^p, \quad (48)$$

where ε_{ij}^p is the plastic strain tensor. The tensile flow stress σ_f is proportionally related to τ *via* the Taylor factor M such that, considering (45)-(47),

$$\sigma_f = M\tau = 0.5M\mu b\sqrt{\rho_{SSD} + \bar{r}\frac{\eta^p}{b}}. \quad (49)$$

Here, $M = 2.9$ for bcc metals. The SSD density ρ_{SSD} can be determined from (49) knowing the relation in uniaxial tension ($\eta = 0$) between the flow stress and the material stress-strain curve as follows

$$\rho_{SSD} = \left(\frac{\sigma_{ref}f(\varepsilon^p)}{0.5M\mu b}\right)^2, \quad (50)$$

where σ_{ref} is a reference stress and $f(\varepsilon^p)$ is a non-dimensional function determined from the uniaxial stress-strain curve. Substituting back into (49), one reaches

$$\sigma_f = \sigma_{ref}\sqrt{f^2(\varepsilon^p) + \ell\eta^p} \quad (51)$$

where ℓ is the intrinsic material length. If the length parameter is set to zero or $f^2(\varepsilon^p)$ outweighs the GND contribution $\ell\eta^p$, the model recovers conventional von Mises plasticity. Once ρ is known, Eq. (30) can be used to estimate the trap density for dislocations. For simplicity, in this implementation only conventional plasticity will be considered and therefore $\rho = \rho_{SSD}$. As with the previous schemes, a rate-dependent term (not considered here) can be implemented using (44).

3. ABAQUS implementation

In the following we shall describe the peculiarities of the finite element implementation in ABAQUS. As in [2, 18, 31, 32], this is achieved by exploiting the analogy with heat transfer and making use of two subroutines: a UMATHT for the diffusion problem and a UMAT for the mechanical problem.

3.1. Analogy to the heat transfer problem

In the absence of a heat source, the energy balance for a stationary solid can be expressed as:

$$\int_V \rho \dot{U}^q dV + \int_S \mathbf{J}^q dS = 0 \quad (52)$$

$$\rho \dot{U}^q = -\nabla \cdot \mathbf{J}^q \quad (53)$$

The heat flux \mathbf{J}^q depends on the temperature gradient according to Fourier's law. And U^q is the internal energy per unit mass, with the superscript q being employed to denote heat related variables. By setting the density equal to 1, the total hydrogen concentration can be regarded as the internal energy per unit mass, see Eq. (24), being both conserved quantities in the global balance. At constant pressure, the variation of energy and temperature can be defined as specific heat capacity c_p :

$$\dot{U}^q = c_p \dot{T} \quad (54)$$

The following relations can be therefore envisaged:

Table 1: Analogy of variables between heat transfer and diffusion analysis

| Heat equation | Mass diffusion equation |
|--|--|
| $\rho c_p \frac{\partial T}{\partial t} + \nabla \cdot \mathbf{J}^q = 0$ | $\frac{\partial C}{\partial t} + \nabla \cdot \mathbf{J} = 0$ |
| $\dot{U}^q = c_p \dot{T}$ | $\frac{\partial C}{\partial t} = \frac{\partial(C_L + C_T)}{\partial t}$ |
| Degree of freedom: T | Degree of freedom: C_L |
| Heat flux: \mathbf{J}^q | Hydrogen flux: \mathbf{J} |
| Heat capacity: c_p | 1 (unity) |
| ρ density | 1 (unity) |

3.2. UMATHT subroutine

The numerical implementation is carried on in ABAQUS by means of a UMATHT subroutine. A number of variables must be defined in the subroutine, whose equivalence to heat transfer and mass diffusion variables are defined in Table 2.

Table 2: Quantities that need to be defined in a UMATHT subroutine

| UMATHT variable | Heat transfer | Mass diffusion |
|-------------------|---|---|
| U | U^q | C |
| DUDT | $\frac{\partial U^q}{\partial T}$ | $\frac{\partial C}{\partial C_L}$ |
| DUDG(NTGRD) | $\frac{\partial U^q}{\partial \nabla T}$ | $\frac{\partial C}{\partial \nabla C_L}$ |
| FLUX(NTGRD) | \mathbf{J}^q | \mathbf{J} |
| DFDT(NTGRD) | $\frac{\partial \mathbf{J}^q}{\partial T}$ | $\frac{\partial \mathbf{J}}{\partial C_L}$ |
| DFDG(NTGRD,NTGRD) | $\frac{\partial \mathbf{J}^q}{\partial \nabla T}$ | $\frac{\partial \mathbf{J}}{\partial \nabla C_L}$ |

Where the variable `NTGRD` is the number of spatial gradients of temperature. One should note that ∇C_L does not need to be computed, as it is given by ABAQUS to the subroutine through the variable `DTEMPDX` (∇T). The subroutine gives as input the following variables at the beginning of the increment: total hydrogen concentration $C(\mathbf{U})$, lattice hydrogen concentration C_L (`TEMP`) and gradient of the lattice hydrogen concentration ∇C_L (`DTEMPDX`). Moreover, it provides as well the incremental lattice hydrogen concentration ΔC_L (`DTEMP`). So, the first step is to work with the current C_L value, which is assigned to a variable `CL`:

`CL=TEMP+DTEMP`

Now, let us consider each term individually. First, we shall define the total hydrogen concentration at the end of the increment, \mathbf{U} . This is given by: (recall that $\Delta a = \dot{a}\Delta t$)

$$C(t + \Delta t) = C(t) + \frac{\partial C}{\partial t} \Delta t = \frac{\partial C}{\partial C_L} \frac{\partial C_L}{\partial t} \Delta t + \frac{\partial C}{\partial C_T} \frac{\partial C_T}{\partial t} \Delta t \quad (55)$$

`U=U+DUDT*DTEMP+DU2`

Here, the variable `DUDT` is addressed below and the variable `DU2` corresponds to the rate-dependent term of the dislocation trapping law; i.e., either zero or the second term in Eqs. (40) or (44). For example, for the model by Krom *et al.* [12] (Section 2.6.2), considering (41) and (42):

$$\text{DU2} \equiv \frac{\partial C}{\partial N_T} \frac{dN_T}{d\varepsilon^p} \frac{\partial \varepsilon^p}{\partial t} = \frac{KC_L}{KC_L + N_L} 29.5 \exp(-5.5\varepsilon^p) N_T \Delta \varepsilon^p \quad (56)$$

While for the case of Dadfarnia *et al.* [14] (Section 2.6.3), the variable DU2 corresponds to the second term in (44); i.e., considering (41) and (43):

$$\text{DU2} \equiv \frac{\partial C}{\partial N_T} \frac{dN_T}{d\rho} \frac{\partial \rho}{\partial t} = \frac{KC_L}{KC_L + N_L} \frac{1}{b} \gamma \Delta \varepsilon^p \quad (57)$$

And one should be careful with the units, as in (43) the dislocation density is given in m^{-2} but we have chosen to work in mm^{-2} instead. In both dislocation-based or ε^p -based dislocation trapping schemes there is an obvious coupling with the mechanical problem. This can be easily addressed in ABAQUS exploiting the fact that the solution-dependent state variables (STATEV) are shared between UMAT and UMATHT subroutines.

Let us consider now the term DUDT, which is given by:

$$\frac{\partial C}{\partial C_L} = \frac{\partial C_L}{\partial C_L} + \sum_i \frac{\partial C_T^{(i)}}{\partial C_L} = 1 + \sum_i \frac{C_T^{(i)} (1 - \theta_T^{(i)})}{C_L} = 1 + \sum_i \frac{K^{(i)} N_L N_T^{(i)}}{(K^{(i)} C_L + N_L)^2} \quad (58)$$

```
DUDT=1.D0+DU DT2
```

```
DUDT2=0.d0
```

```
do k1=1,ntraps
```

```
  DUDT2=DUDT2+xNt(k1)*xK(k1)*xN1/((xK(k1)*CL+xN1)**2.d0)
```

```
end do
```

where `ntraps` is the number of traps, $\text{xNt} \equiv N_T^{(i)}$, $\text{xK} \equiv K^{(i)}$, and $\text{xN1} \equiv N_L$. On the other hand the term DUDG, equivalent to $\partial C_L / \partial \nabla C_L$, is zero. Each component of the flux \mathbf{J} (FLUX) is given by:

$$\mathbf{J} = -D \nabla C_L + \frac{D}{RT} C_L \bar{V}_H \nabla \sigma_H \quad (59)$$

```
FLUX(i)=-D*DTEMDX(i)+D*CL*Vh*sig(i)/(R*T)
```

where `sig(i)` is the gradient of the hydrostatic stress, $\nabla \sigma_H$, whose computation will be addressed below. Accordingly, the term DFDT reads,

$$\frac{\partial \mathbf{J}}{\partial C_L} = \frac{D}{RT} \bar{V}_H \nabla \sigma_H \quad (60)$$

```
DFDT(i)=D*Vh*sig(i)/(R*T)
```

and in both the definition of the flux and its derivative, one should be careful with the units when defining the gas constant (R). The term $\bar{V}_H \sigma_H / (RT)$ must be non-dimensional. Assuming that the stresses are given in MPa (N/mm²), then $R = 8314$ N mm/(mol K). Note that the gas constant also appears in the calculation of the equilibrium constant K , see (11). This means that the binding energy, W_B , should be given in units of N mm/mol (remember, 1 kJ/mol \equiv 10⁶ N mm/mol).

Finally, it remains to define the variable DFDG, given as follows:

$$\frac{\partial \mathbf{J}}{\partial \nabla C_L} = -D \mathbf{I} \quad (61)$$

DFDG(i, i)=-D

with \mathbf{I} being the identity matrix, as only the diagonal terms in $\frac{\partial \mathbf{J}}{\partial \nabla C_L}$ are non-zero (only $\nabla^x C_L$ is involved in the x component of \mathbf{J}).

In addition to the quantities required by ABAQUS, one might chose to define additional quantities for visualisation such as (e.g.) the trapped hydrogen concentration, as per (15).

3.2.1. General case: θ_L not much smaller than 1

Note that, if the approximation $\theta_L \ll 1$ cannot be assumed (e.g., fcc metals), then (14) does not hold. Consequently, the computation of DUDT will be affected, and should be re-formulated as:

$$\frac{\partial C}{\partial C_L} = \frac{\partial C_L}{\partial C_L} + \sum_i \frac{\partial C_T^{(i)}}{\partial C_L} = 1 + \sum_i \frac{K^{(i)} N_L N_T^{(i)}}{((K^{(i)} - 1) C_L + N_L)^2} \quad (62)$$

DUDT=1.D0+DUDT2

DUDT2=0.d0

do k1=1, ntraps

DUDT2=DUDT2+xNt(k1)*xK(k1)*xN1/(((xK(k1)-1)*CL+xN1)**2.d0)

end do

Also, for computing the concentration in each trap $C_T^{(i)}$, one cannot longer use (15), which should instead read:

$$C_T^{(i)} = \frac{C_L N_T^{(i)} K^{(i)}}{N_L + (K^{(i)} - 1) C_L} \quad (63)$$

3.3. Gradient of the hydrostatic stress

The mechanical behaviour of the solid will be described using conventional plasticity and will not be elaborated here. A user material (UMAT) subroutine is used, which corresponds to the UMAT for power law hardening plasticity available to download at www.imperial.ac.uk/mechanics-materials/codes/ and www.empaneda.com/codes/; the reader is referred to the accompanying documentation for details. What will be addressed here is the computation of hydrostatic stress gradient, a feature specific to this problem and thus not available in the original UMAT subroutine.

The quantity $\nabla\sigma_H$ is computed using a relatively simple differentiation scheme at the element level. First, the magnitude of σ_H is interpolated through its values at the Gauss points in the isoparametric space and afterwards $\nabla\sigma_H$ is computed by differentiation of the shape functions. This procedure is outlined below for the particular case of a plane strain quadrilateral element with 8 nodes and 4 integration points, extension to other types of elements can be performed in a relatively straightforward manner. More sophisticated approaches exist and the reader is referred to Ref. [19] and the associated code for alternatives.

The hydrostatic stress values within the element can be readily obtained from its values at the Gauss integration points $(\sigma_H)_k$

$$\sigma_H = \sum_{k=1}^4 N'_k(x, y) (\sigma_H)_k \quad (64)$$

where $N'_k(x, y)$ is the interpolation function in global coordinates. By performing the classic isoparametric mapping, the coordinate transformation is:

$$x = \sum_{k=1}^4 N_k(\xi, \eta) x_k \quad (65)$$

$$y = \sum_{k=1}^4 N_k(\xi, \eta) y_k \quad (66)$$

where $N_k(\xi, \eta)$ is the shape function vector. For convenience, the interpolation function in local coordinates takes the same form as the shape functions

and (64) becomes:

$$\sigma_H = \sum_{k=1}^4 N_k(\xi, \eta) (\sigma_H)_k \quad (67)$$

Accordingly, linear shape functions are adopted,

$$N_i = \frac{1}{4} (1 + \xi_i \xi) (1 + \eta_i \eta) \quad (68)$$

with ξ_i and η_i denoting the integration point coordinates in the isoparametric space.

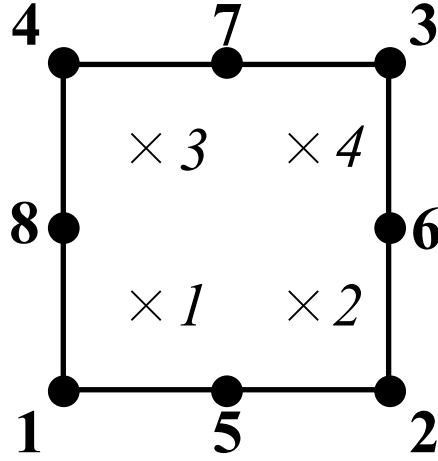


Figure 2: Nodal and integration point numbering adopted for a quadrilateral plane strain quadratic finite element

The numbering scheme in this Gauss point-based interpolation is depicted in Fig. 2. The differentiation of the shape functions readily follows:

$$\frac{\partial N_i}{\partial \xi} = \frac{1}{4} \xi_i (1 + \eta \eta_i) \quad (69)$$

$$\frac{\partial N_i}{\partial \eta} = \frac{1}{4} \eta_i (1 + \xi \xi_i) \quad (70)$$

Which, by means of the chain rule, can be easily converted to the global coordinate system,

$$\begin{bmatrix} \frac{\partial N_k}{\partial x} \\ \frac{\partial N_k}{\partial y} \end{bmatrix} = J^{-1} \begin{bmatrix} \frac{\partial N_k}{\partial \xi} \\ \frac{\partial N_k}{\partial \eta} \end{bmatrix} \quad (71)$$

with J being the Jacobian matrix:

$$J = \frac{\partial(x, y)}{\partial(\xi, \eta)} = \begin{bmatrix} \frac{\partial x}{\partial \xi} & \frac{\partial y}{\partial \xi} \\ \frac{\partial x}{\partial \eta} & \frac{\partial y}{\partial \eta} \end{bmatrix} = \begin{bmatrix} \sum_{k=1}^4 \frac{\partial N_k}{\partial \xi} x_k & \sum_{k=1}^4 \frac{\partial N_k}{\partial \xi} y_k \\ \sum_{k=1}^4 \frac{\partial N_k}{\partial \eta} x_k & \sum_{k=1}^4 \frac{\partial N_k}{\partial \eta} y_k \end{bmatrix} \quad (72)$$

The hydrostatic stress gradient $\nabla \sigma_H$ is then computed as:

$$(\nabla \sigma_H)_x = \sum_{i=1}^4 \frac{\partial N_i}{\partial x} (\sigma_H)_i \quad (73)$$

$$(\nabla \sigma_H)_y = \sum_{i=1}^4 \frac{\partial N_i}{\partial y} (\sigma_H)_i \quad (74)$$

This operations take place inside of the UMAT subroutine, and the information is then passed to the UMATHHT. Both UMAT and UMATHHT are integration point level subroutines but it is obvious that the computation of $\nabla \sigma_H$ requires access to the magnitude of σ_H in all the integration points of the elements. This is achieved by means of a Fortran module (the modern version of common blocks).

4. Usage instructions

We proceed to showcase the use of the subroutine by validating with an example from the literature; specifically, Fig. 3 of the multi-trap analysis by Dadfarnia *et al.* [14].

4.1. Abaqus/CAE and input file

The first step is to create the model in Abaqus/CAE. The procedure is the same as with standard Abaqus models with the following subtleties:

- Depending on the trapping scheme used, some unit sensitive variables have been hard-coded assuming that mm is choice of unit for length.
- The material has to be defined as a user material, of the thermomechanical type, with a number of solution-dependent variables. (General \rightarrow Depvar: 16 & General \rightarrow User Material - Thermomechanical). The material properties are described below. Also, the density must be defined, and given the value 1.

- The loading step is of the type coupled temperature-displacement. This step type assumes an instantaneous application of the boundary conditions, which might be suitable for the hydrogen-related ones but potentially not for the mechanical ones. One option is to change the loading to ramp-type and then define a constant amplitude to be associated with the hydrogen boundary conditions. Another option is to make use of a DISP subroutine. Also, recall that the total step time is not a pseudo-time. If the time stepping is chosen to be automatic, the maximum allowable nodal temperature change in an increment must be specified (`deltmx`; ΔT_{max}); the choice is a trade-off between convergence rates and precision.
- SDV, Solution dependent state variables, have to be requested as Field Output (as well as displacement, nodal temperatures, reaction forces and other relevant quantities). (Field Output Request - State/Field/User/Time: SDV, Solution dependent state variables)
- The element type has to be substituted by a coupled mechanical-thermal element (i.e., CPE8RT instead of CPE8R).
- Initial and boundary conditions related to hydrogen transport are defined as temperature initial or boundary conditions (DOF11).

The mechanical and thermal properties are respectively listed in Tables 3 and 4. The mechanical behaviour is characterised by conventional von Mises plasticity, with an isotropic power law hardening as follows:

$$\sigma = \sigma_Y \left(1 + \frac{E\varepsilon^p}{\sigma_Y} \right)^N \quad (75)$$

where σ_Y is the initial yield stress, E is Young's modulus and N is the strain hardening exponent. If the model by Fernandez-Sousa et al. [9] is used, the density of statistically stored dislocations is hard-coded assuming mm as length unit and a bcc material. MPa units should be used for E and σ_Y .

Table 3: List of user defined properties for the UMAT subroutine.

| PROPS | Variables UMAT |
|-------|-----------------------------------|
| 1 | E - Young's modulus |
| 2 | ν - Poisson's ratio |
| 3 | σ_Y - Initial yield stress |
| 4 | N - Strain hardening exponent |

The thermal properties are related to the mass diffusion problem. The code is arranged in a way that can be used with an arbitrary number of traps n ; the number of traps is automatically recognised depending on the number of PROPS defined on the thermal side. PROPS(2) is a flag variable that defines the type of analysis that is going to be conducted. If equal to 0, all the trap densities are made equal to 0, and the analysis considers lattice diffusion only, overriding the $W_B^{(i)}$ and $N_T^{(i)}$ definitions. If equal to 1, the analysis makes zero W_B^1 and N_T^1 , which correspond to the binding energy and the trap density of the first trap type. The first trap type is associated to dislocations to facilitate the use of the dislocation trapping schemes described in Section 2.6. The scheme by Kunnick and Johnson [20] & Sofronis and McMeeking [10] (Section 2.6.1) is activated if the flag variable equals 2. When equal to 3, we use the scheme by Krom et al. [12], also based on Ref. [20] but including a rate-dependent term (Section 2.6.2). The dislocation-based model by Sofronis and co-workers (Section 2.6.3) is activated with PROPS(2)=4 - this scheme will be used in this verification example, following Dadfarnia *et al.* [14]. Finally, PROPS(2)=5 activates the model by Fernandez-Sousa et al. [9] neglecting the influence of plastic strain gradients and GNDs.

Table 4: List of user defined properties for the UMATHHT subroutine for the case of three trap types.

| PROPS | Variables UMATHHT |
|-------|---|
| 1 | D - Lattice diffusion coefficient |
| 2 | Flag: 0 - $C_T = 0$; 1 - $C_T^{(1)} = 0$; 2 - [10]; 3 - [12]; 4 - [14]; 5 - [9] |
| 3 | $W_B^{(1)}$ - Binding energy, trap type 1 (dislocations) |
| 4 | $N_T^{(1)}$ - Trap density, trap type 1 (dislocations) |
| 5 | $W_B^{(2)}$ - Binding energy, trap type 2 |
| 6 | $N_T^{(2)}$ - Trap density, trap type 2 |
| 7 | $W_B^{(3)}$ - Binding energy, trap type 3 |
| 8 | $N_T^{(3)}$ - Trap density, trap type 3 |

The remaining PROPS are associated with the binding energy and the trap density of each trap type. First, dislocations must be defined. As many trap types as required are defined afterwards in any order; Table 4 shows as example the case where 3 trap types are considered. The trap density should be defined in units of sites/mm³ and the binding energies should be given in Nmm/mol, as discussed in Section 3.2.

The choices of solution-dependent variables SDVs are motivated by the history-dependent nature of the problem and visualisation. A total of 16 SDVs are considered in the case of a 3-trap system, as listed in Table 5.

| Variable | SDVs numbering |
|--|------------------|
| Axial elastic strains - $\varepsilon_{11}^e, \varepsilon_{22}^e, \varepsilon_{33}^e$ | SDV1, SDV2, SDV3 |
| Shear elastic strains - ε_{12}^e | SDV4 |
| Axial plastic strains - $\varepsilon_{11}^p, \varepsilon_{22}^p, \varepsilon_{33}^p$ | SDV5, SDV6, SDV7 |
| Shear plastic strain - ε_{12}^p | SDV8 |
| Equivalent plastic strain - ε^p | SDV9 |
| Incremental equivalent plastic strain - $\Delta\varepsilon^p$ | SDV10 |
| Dislocation density (SSDs) - $N_T = \rho$ | SDV11 |
| Hydrogen concentration on trap 1 (dislocations) - $C_T^{(1)}$ | SDV12 |
| Hydrogen concentration on trap 2 - $C_T^{(2)}$ | SDV13 |
| Hydrogen concentration on trap 3 - $C_T^{(3)}$ | SDV14 |
| Trapped hydrogen concentration - C_T | SDV15 |
| Total hydrogen concentration - C | SDV16 |

Table 5: List of solution dependent state variables for the case of three traps types.

4.2. Boundary value problem and results

We validate our implementation with the crack tip hydrogen distributions calculated by Dadfarnia *et al.* [14]. As in Ref. [14], a boundary layer model is used. Hence, as described in Fig. 3, the crack region is contained by a circular zone and a remote Mode I load K_I is applied by prescribing the horizontal u_x and vertical u_y displacement components of the nodes at the remote circular boundary:

$$u_x(r, \theta) = K_I \frac{1 + \nu}{E} \sqrt{\frac{r}{2\pi}} \cos\left(\frac{\theta}{2}\right) (3 - 4\nu - \cos\theta) \quad (76)$$

$$u_y(r, \theta) = K_I \frac{1 + \nu}{E} \sqrt{\frac{r}{2\pi}} \sin\left(\frac{\theta}{2}\right) (3 - 4\nu - \cos\theta) \quad (77)$$

where r and θ denote the radial and angular coordinates of a polar coordinate system centred at the crack tip. Plane strain conditions and finite deformations are considered. An initial crack tip blunting radius is defined $r_0 = 0.5 \mu\text{m}$, rendering an initial crack tip opening displacement of $b_0 = 1 \mu\text{m}$. The outer radius is chosen to be 300,000 times larger than r_0 .

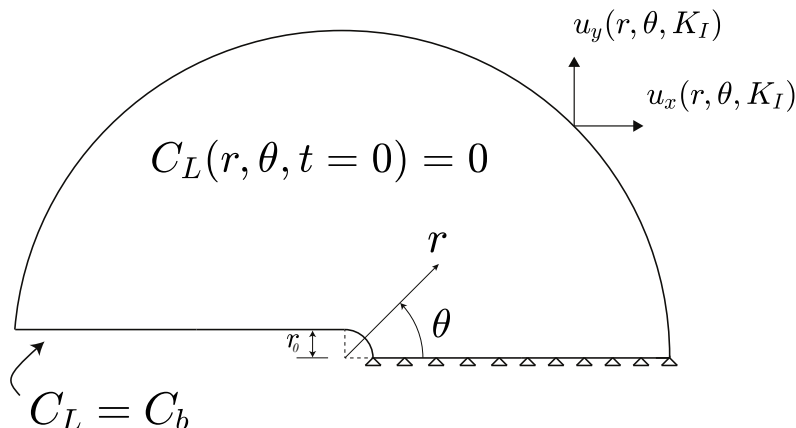


Figure 3: Sketch of the numerical model: boundary layer formulation, with mechanical and diffusion boundary conditions.

The sample is not pre-charged and accordingly an initial condition is defined: $C_L(t = 0) = 0$. In Ref. [14], the hydrogen pressure ramps from 0 to 15 MPa in one second, leading to a concentration of $C_b = 2.659 \times 10^{13}$ H atoms/mm³ at a time of $t = 1$ s. Thus, the step is defined as ramp type. The mechanical boundary conditions are introduced by means of a DISP subroutine, the load is ramped up to $t = 1$ s, where it reaches a magnitude of $K_I = 30 \text{ MPa}\sqrt{m}$.

The mechanical properties read $E = 201,880 \text{ MPa}$, $\nu = 0.3$, $\sigma_Y = 595 \text{ MPa}$, and $N = 0.059$. The lattice diffusion coefficient equals $D = 0.01271 \text{ mm}^2/\text{s}$ and three types of traps are considered. (1) Dislocations, with a binding energy of $W_B^{(d)} = 20.2 \times 10^6 \text{ N mm/mol}$ and a trap density given by the dislocation-based scheme of Sofronis and co-workers (PROPS(2)=4, Section 2.6.3). (2) Grain boundaries, with $W_B^{(c)} = 58.6 \times 10^6 \text{ N mm/mol}$ and $N_T^{(c)} = 8.464 \times 10^{13} \text{ sites/mm}^3$. And (3) carbides, with $W_B^{(c)} = 11.5 \times 10^6 \text{ N mm/mol}$ and $N_T^{(c)} = 8.464 \times 10^{17} \text{ sites/mm}^3$. Note that we introduce W_B as a positive number.

The results obtained after a time of $t = 1$ s are shown in Fig. 4 in terms of the hydrogen concentration ahead of the crack tip for the various trap types. The results exhibit a very good agreement with those obtained by Dadfarnia *et al.* [14]. One should note that the files provided do not incorporate the chemical strains considered in Ref. [14]. Also, the value of Burgers vector

used in Ref. [14] is slightly different than the one adopted here (0.2725 versus 0.202 nm), and the density of lattice sites is given assuming tetrahedral site occupancy ($\beta = 6$ [12]) and not $\beta = 1$. The user would have to make those changes to reproduce the results of the figure. In addition, defining a small initial concentration ($C_0 = 1 \times 10^{10}$ H atoms/mm³) makes the solution more stable [10], enabling achieving accurate results with a higher value of ΔT_{max} (i.e., using larger time increments).

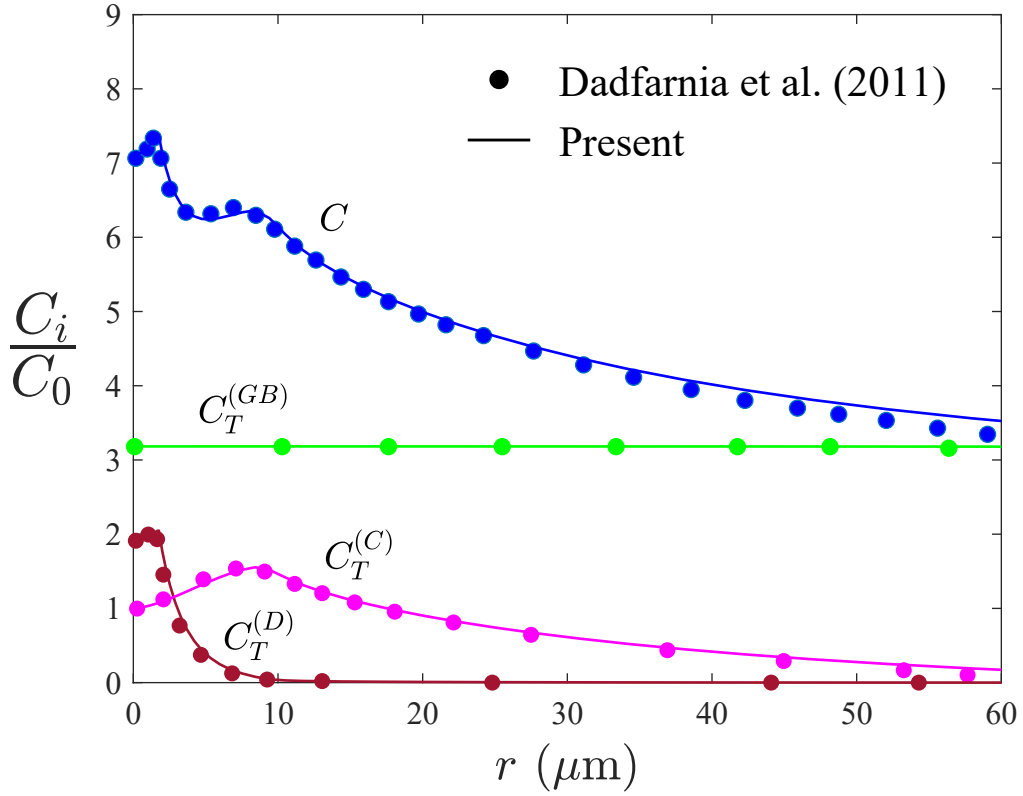


Figure 4: Normalised hydrogen concentration ahead of the crack after a time of $t = 1$ s: total C (lattice and trapped), trapped at carbides $C_T^{(C)}$, trapped at dislocations $C_T^{(D)}$, and trapped at grain boundaries $C_T^{(GB)}$. Symbols denote the (digitized) results by Dadfarnia *et al.* [14] while lines denote the predictions of the present implementation.

5. Conclusions

If the code or the documentation provided here are useful please cite:

R. Fernández-Sousa, C. Betegón, E. Martínez-Pañeda. Analysis of the influence of microstructural traps on hydrogen assisted fatigue. *Acta Materialia* 199: pp. 253-263 (2020)

Do not hesitate to contact for further clarifications.

6. Acknowledgments

E. Martínez-Pañeda acknowledges financial support from EPSRC funding under grant No. EP/R010161/1 and from the UKCRIC Coordination Node, EPSRC grant number EP/R017727/1, which funds UKCRIC's ongoing coordination.

References

- [1] R. P. Gangloff, Hydrogen-assisted Cracking, in: I. Milne, R. Ritchie, B. Karihaloo (Eds.), *Comprehensive Structural Integrity* Vol. 6, Elsevier Science, New York, NY, 2003, pp. 31–101.
- [2] S. del Busto, C. Betegón, E. Martínez-Pañeda, A cohesive zone framework for environmentally assisted fatigue, *Engineering Fracture Mechanics* 185 (2017) 210–226.
- [3] E. Martínez-Pañeda, C. F. Niordson, R. P. Gangloff, Strain gradient plasticity-based modeling of hydrogen environment assisted cracking, *Acta Materialia* 117 (2016) 321–332.
- [4] E. Martínez-Pañeda, S. del Busto, C. F. Niordson, C. Betegón, Strain gradient plasticity modeling of hydrogen diffusion to the crack tip, *International Journal of Hydrogen Energy* 41 (24) (2016) 10265–10274.
- [5] E. Martínez-Pañeda, Z. D. Harris, S. Fuentes-Alonso, J. R. Scully, J. T. Burns, On the suitability of slow strain rate tensile testing for assessing hydrogen embrittlement susceptibility, *Corrosion Science* 163 (2020) 108291.
- [6] P. K. Kristensen, C. F. Niordson, E. Martínez-Pañeda, A phase field model for elastic-gradient-plastic solids undergoing hydrogen embrittlement, *Journal of the Mechanics and Physics of Solids* 143 (2020) 104093.

- [7] D. Li, R. P. Gangloff, J. R. Scully, Hydrogen Trap States in Ultrahigh-Strength AERMET 100 Steel, *Metallurgical and Materials Transactions A: Physical Metallurgy and Materials Science* 35 A (3) (2004) 849–864.
- [8] A. Turnbull, Perspectives on hydrogen uptake, diffusion and trapping, *International Journal of Hydrogen Energy* 40 (47) (2015) 16961–16970.
- [9] R. Fernández-Sousa, C. Betegón, E. Martínez-Pañeda, Analysis of the influence of microstructural traps on hydrogen assisted fatigue, *Acta Materialia* 199 (2020) 253–263.
- [10] P. Sofronis, R. M. McMeeking, Numerical analysis of hydrogen transport near a blunting crack tip, *Journal of the Mechanics and Physics of Solids* 37 (3) (1989) 317–350.
- [11] C. V. Di Leo, L. Anand, Hydrogen in metals: A coupled theory for species diffusion and large elastic-plastic deformations, *International Journal of Plasticity* 43 (2013) 42–69.
- [12] A. H. M. Krom, R. W. J. Koers, A. Bakker, Hydrogen transport near a blunting crack tip, *Journal of the Mechanics and Physics of Solids* 47 (4) (1999) 971–992.
- [13] P. Novak, R. Yuan, B. P. Somerday, P. Sofronis, R. O. Ritchie, A statistical, physical-based, micro-mechanical model of hydrogen-induced intergranular fracture in steel, *Journal of the Mechanics and Physics of Solids* 58 (2) (2010) 206–226.
- [14] M. Dadfarnia, P. Sofronis, T. Neeraj, Hydrogen interaction with multiple traps: Can it be used to mitigate embrittlement?, *International Journal of Hydrogen Energy* 36 (16) (2011) 10141–10148.
- [15] R. A. Oriani, P. H. Josephic, Equilibrium Aspects of Hydrogen Induced Cracking of Steels, *Acta Metallurgica* 22 (1974) 1065–1074.
- [16] E. Martínez-Pañeda, A. Díaz, L. Wright, A. Turnbull, Generalised boundary conditions for hydrogen transport at crack tips, *Corrosion Science* 173 (2020) 108698.
- [17] A. Díaz, I. I. Cuesta, E. Martínez-Pañeda, J. M. Alegre, Influence of charging conditions on simulated temperature-programmed desorption

- for hydrogen in metals, *International Journal of Hydrogen Energy* 45 (2020) 23704–23720.
- [18] A. Díaz, J. M. Alegre, I. I. Cuesta, Coupled hydrogen diffusion simulation using a heat transfer analogy, *International Journal of Mechanical Sciences* 115-116 (2016) 360–369.
 - [19] E. Martínez-Pañeda, A. Golahmar, C. F. Niordson, A phase field formulation for hydrogen assisted cracking, *Computer Methods in Applied Mechanics and Engineering* 342 (2018) 742–761.
 - [20] A. J. Kumnick, H. H. Johnson, Deep trapping states for hydrogen in deformed iron, *Acta Metallurgica* 28 (1) (1980) 33–39.
 - [21] R. Falkenberg, W. Brocks, W. Dietzel, I. Scheider, Modelling the effect of hydrogen on ductile tearing resistance of steels, *International Journal of Materials Research* 101 (8) (2010) 989–996. doi:10.3139/146.110368.
 - [22] E. Martínez-Pañeda, C. Betegón, Modeling damage and fracture within strain-gradient plasticity, *International Journal of Solids and Structures* 59 (2015) 208–215.
 - [23] E. Martínez-Pañeda, V. S. Deshpande, C. F. Niordson, N. A. Fleck, The role of plastic strain gradients in the crack growth resistance of metals, *Journal of the Mechanics and Physics of Solids* 126 (2019) 136–150.
 - [24] J. J. Gilman, *Micromechanics of Flow in Solids*, McGraw-Hill, New York, NY, 1969.
 - [25] P. Sofronis, Y. Liang, N. Aravas, Hydrogen induced shear localization of the plastic flow in metals and alloys, *Eur. J. Mech. A/Solids* 20 (2001) 857–872.
 - [26] J. R. Low, A. M. Turkalo, Slip band structure and dislocation multiplication in silicon-iron crystals, *Acta Metallurgica* 10 (3) (1962) 215–227.
 - [27] G. I. Taylor, Plastic strain in metals, *Journal of the Institute of Metals* 62 (1938) 307–324.
 - [28] E. Martínez-Pañeda, C. F. Niordson, On fracture in finite strain gradient plasticity, *International Journal of Plasticity* 80 (2016) 154–167.

- [29] E. Martínez-Pañeda, S. Natarajan, S. Bordas, Gradient plasticity crack tip characterization by means of the extended finite element method, *Computational Mechanics* 59 (2017) 831–842.
- [30] H. Gao, Y. Hang, W. D. Nix, J. W. Hutchinson, Mechanism-based strain gradient plasticity - I. Theory, *Journal of the Mechanics and Physics of Solids* 47 (6) (1999) 1239–1263.
- [31] C.-S. Oh, Y.-J. Kim, K.-B. Yoon, Coupled Analysis of Hydrogen Transport using ABAQUS, *Journal of Solid Mechanics and Materials Engineering* 4 (7) (2010) 908–917.
- [32] O. Barrera, E. Tarleton, H. W. Tang, A. C. F. Cocks, Modelling the coupling between hydrogen diffusion and the mechanical behaviour of metals, *Computational Materials Science* 122 (2016) 219–228.